Journal of Solid State Chemistry 184 (2011) 615–623

Contents lists available at ScienceDirect

Journal of Solid State Chemistry

journal homepage: www.elsevier.com/locate/jssc

Optimization of processing parameters on the controlled growth of ZnO nanorod arrays for the performance improvement of solid-state dye-sensitized solar cells

Yi-Mu Lee [a,*], Hsi-Wen Yang [b]

[a] Department of Electronic Engineering, National United University, MiaoLi 36003, Taiwan
[b] Department of Materials Science and Engineering, National United University, MiaoLi 36003, Taiwan

ARTICLE INFO

Article history:
Received 25 October 2010
Received in revised form
7 December 2010
Accepted 17 January 2011
Available online 26 January 2011

Keywords:
Chemical bath deposition
ZnO
Nanorod arrays
Electrical properties
Heterojunction electrode

ABSTRACT

High-transparency and high quality ZnO nanorod arrays were grown on the ITO substrates by a two-step chemical bath deposition (CBD) method. The effects of processing parameters including reaction temperature (25–95 °C) and solution concentration (0.01–0.1 M) on the crystal growth, alignment, optical and electrical properties were systematically investigated. It has been found that these process parameters are critical for the growth, orientation and aspect ratio of the nanorod arrays, showing different structural and optical properties. Experimental results reveal that the hexagonal ZnO nanorod arrays prepared under reaction temperature of 95 °C and solution concentration of 0.03 M possess highest aspect ratio of ~21, and show the well-aligned orientation and optimum optical properties. Moreover the ZnO nanorod arrays based heterojunction electrodes and the solid-state dye-sensitized solar cells (SS-DSSCs) were fabricated with an improved optoelectrical performance.

1. Introduction

ZnO is an attracting nanomaterial exhibiting high-transparency in the visible region, near-UV emission, magnetic, piezoelectric and high-conductivity properties. It has a wide and direct band gap (3.37 eV), large binding energy (60 meV) [1,2] and excellent chemical, thermal and mechanical stability [3,4]. Nanostructured ZnO materials have received intensive research for wide applications in light-emitting diodes [5], gas/chemical sensors [6,7], thin-film transistors [8], micro/nanoelectronic devices [9,10] and photovoltaic cells [11,12–14]. The applications of nanostructures in nanoelectronic devices strongly depend on the shape, morphology and size. Thus, realizing the controlled growth of well-aligned nanostructures is a critical step for broadening their applications in nanodevices. Up to now, many kinds of ZnO nanostructures have been synthesized by various deposition technologies. Thin films of ZnO can be produced by rf magnetron sputtering [15,16], pulsed laser deposition (PLD) [17] and sol–gel process [5,18]. Several 1-D ZnO nanostructures, including nanobelts, nanowires, nanorods, nanotubes, nanonails and nanoflowers, have been synthesized by different growth techniques such as chemical bath deposition [19], spray pyrolysis [20], vapor phase transport [21], sol–gel [22] and hydrothermal method [23]. Indeed it has been shown that the electron transport is enhanced in the 1-D ZnO nanostructures [24–26]. Among the above process techniques, chemical bath deposition (CBD) is of particular interest for the broad applications in large-area fabrication and low-temperature process, which are compatible with plastic substrates for the fabrication of flexible electronics.

Studies on ZnO nanomaterials have shown that the morphology, alignment, film thickness, shape and dimension of the nanostructures can be controlled by changing the process parameters, then the material and optical properties can be modulated [27–30]. The effects of post heat-treatment temperatures on the optical and electrical properties of ZnO branched nanorods have been discussed [31]. It was concluded that the ZnO samples received thermal-treatment at 400 °C possess high optical transmittance (>90%), great coverage and very low resistivity ($\rho = 3.2 \times 10^{-3}\ \Omega$ cm). Also, it has been found that the diameter of flower-like ZnO nanorods is proportional to the concentration of the reactant, while the ZnO length is inversely proportional to the concentration of the reactant [30]. Yang et al. [32] has presented an effective way to control the ZnO particle density of the pretreated Si substrate during CBD, and found that the diameter of ZnO nanorod arrays decreased with an increasing ZnO particle density. Further, it has been found that the density of ZnO nanorod arrays on ITO-glass is strongly dependent on the duration of initial seed deposition; higher density of nanorod arrays

* Corresponding author. Fax: +886 37 362809
E-mail address: ymlee@nuu.edu.tw (Y.-M. Lee).

0022-4596/$ - see front matter © 2011 Elsevier Inc. All rights reserved.
doi:10.1016/j.jssc.2011.01.021

was obtained for longer deposition time [33]. It has also been reported that the seed layer have an influence on the density [3] and the growth direction [34] of the following ZnO nanostructures. Additionally, the crystal morphological transition of ZnO nanostructures by a hydrothermal deposition on the zinc foil has been investigated [35]. This paper reported the transition of the ZnO nanorod arrays from sharp to flat facets by increasing the growing reaction time and the concentration of zinc precursor. The ZnO nanorods have been synthesized with a hydrothermal method; the experimental results show that the UV emission was greatly improved with an increase in crystal size and the change in the optical properties was observed after receiving post-annealing at different atmospheres [36]. ZnO nanowires were synthesized by the CVD method, and it was found that the *I–V* behaviors could be affected by the effective barrier height at the interface state, which depends on the diameter of the nanowires [37]. Suh et al. [14] and Greene et al. [38] both mentioned that the growth temperature for the Si substrate and the conducting glass is different, and is another key factor for the vertical growth of ZnO nanowires. In the study by Rakhshani [39], the length of electrodeposited ZnO rods from a $ZnCl_2$ route can be controlled by the deposition time, whereas the influence on the diameter is more complicated depending on all the process parameters and the substrate type as well.

Recently ZnO nanostructures implemented in electrolyte-DSSCs on the Si substrate have been realized; the results revealed that the branched structure has higher surface area than the pillar-shaped structure of ZnO nanowires, leading to the improvement of light harvesting, photocurrent and the overall energy conversion efficiency (from 0.34% to 0.46%) [14]. However, a few study with further discussion and experimental data were reported for the solar cells with oxide junctions. More research is required to complete the understanding of the controlled growth of the oxide nanostructures for the performance improvement of solid-state DSSCs.

In the present paper, we report the controllable growth of high-transparency and low-resistivity ZnO nanorod arrays through a simple and low-temperature two-step CBD method. The effects of process parameters, reaction temperature and solution concentration, on the material, alignment and optical properties of ZnO were investigated in details. Furthermore, the ZnO nanorod arrays and n-ZnO/p-NiO heterojunction electrode with optimum material and electrical properties were successfully implemented in the solid-state dye-sensitized solar cells to improve the photovoltaic performance.

2. Experimental

2.1. Growth of ZnO nanostructures

Indium tin oxide (ITO) coated glass (AUO Co., Ltd.) was used as transparent conducting substrate with the sheet resistance of 7 Ω/cm. The ITO glasses were initially cleaned with wet chemical cleaning as reported in detail in our previous studies [40]. The chemical bath deposition (CBD) process of ZnO nanorods consist of two steps: (1) deposition of ZnO seeding layer and (2) ZnO nanorod arrays by CBD growth in aqueous solution. All the aqueous solutions were prepared using distilled water. For the deposition of seeding layer, the ITO substrates were dipped in 500 ml aqueous solution containing zinc acetate-2-hydrate [$Zn(CH_3COO)_2 \cdot 2H_2O$] (99% purity, Showa) mixed with hexamethylenetetramine ($C_6H_{12}N_4$, HMTA, 99.5% purity, Riedel-de Haen). The prepared concentration of zinc acetate solution varies from 0.01 to 0.1 M. The role of HMTA is to provide the hydroxide ions (OH^-) and ammonia (NH_3) in the solution [32]. The above process was repeated twice for the above process, and then dried in an oven at 100 °C for 10 min to grow a ZnO seeding layer. The thickness of the seeded layer is around 170 nm and its structural properties have been characterized in our previous studies [31]. In the following, the seeded substrates were then immersed into the same zinc acetate solution. Through the CBD reaction, the pH of the solution was set at 7.5 by adding NH_3OH to the zinc acetate solution. The reaction temperature was maintained at 25, 50, 75 and 95 °C and the reaction time was set to be 3 h. After the CBD growth, all samples received thermal-treatment at 400 °C for 1 h, using an electronic furnace.

2.2. Materials and optical characterization

The morphology and the growth property of the ZnO nanostructures were studied by a field emission scanning electron microscopy (SEM; JEOL model JSM-6700 F, 10 kV). X-ray diffraction (XRD) and energy-dispersive X-ray (EDX) analysis using the Cu$K\alpha$ line were employed to characterize the crystalline structure and the stoichiometric value of the synthesized ZnO samples, respectively. UV–vis spectra were obtained from PerkinElmer Lambda 20 UV/vis/NIR spectrometer.

2.3. Fabrication and I–V measurement of ZnO/NiO heterojunction and DSSC

The n-type ZnO nanorod arrays were first grown on an ITO substrate and then p-type NiO was spin coated onto the n-ZnO/ITO by a spin coater to form the heterojunction electrode. The p-type NiO with thickness of ~170 nm was prepared by the sol–gel process [40]. The coated NiO thin films were dried at 100 °C for 10 min and then the ZnO/NiO heterojunction received thermal-treatment at 400 °C for 1 h. As an upper electrode, gold was deposited by sputtering. Meanwhile, another ITO-glass and the sample were clamped together with two clips. The active area of the resulting device was adjusted to $1.0 \times 1.5\ cm^2$. Fig. 1 illustrates a completed solid-state DSSC structure, which is an interpenetrated network structure facilitating the electron and hole transportation [41]. The current–voltage characteristics of the electrodes were recorded at room temperature using an electrochemical workstation (Jiehan 5000). Then ZnO/NiO heterojunction based solid-state dye-sensitized solar cells (SS-DSSCs)

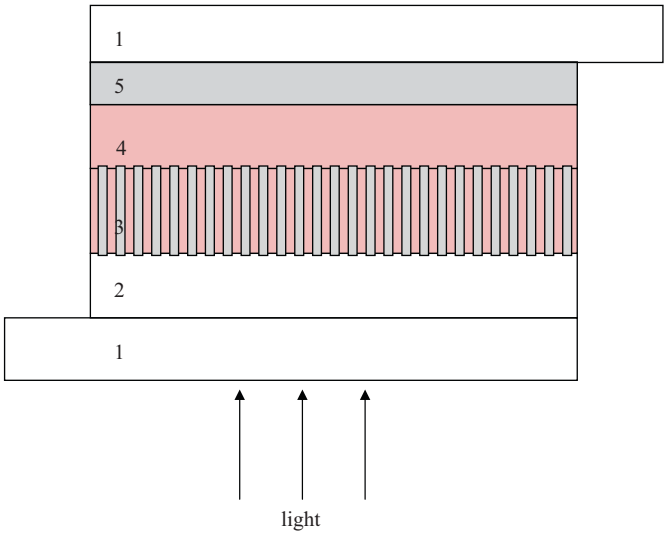

Fig. 1. A schematic illustration of the solid-state DSSCs: (1) ITO-glass; (2) seed layer; (3) dye-sensitized ZnO nanorod arrays; (4) dye-sensitized p-type NiO film; and (5) Au counter electrode.

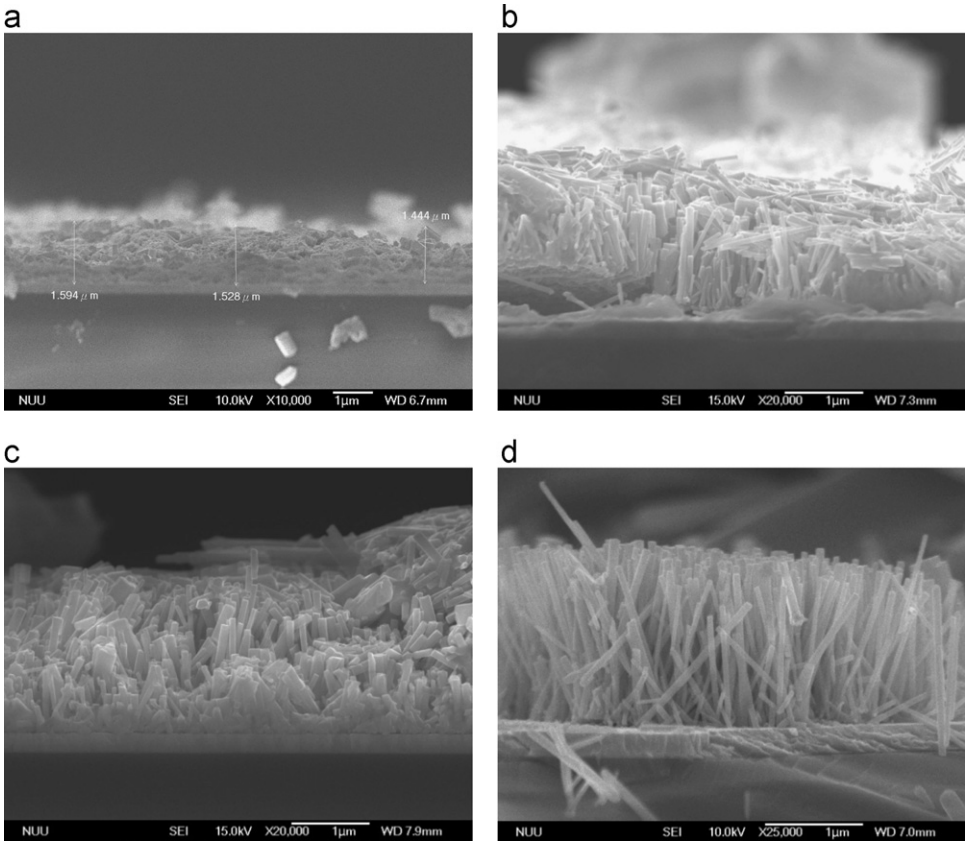

Fig. 2. SEM cross-section images: growth of ZnO nanorods and nanorod arrays as a function of CBD reaction temperatures. (Deposition time: 3 h; solution concentration: 0.03 M.) (a) 25°C, (b) 50°C, (c) 75°C and (d) 95°C.

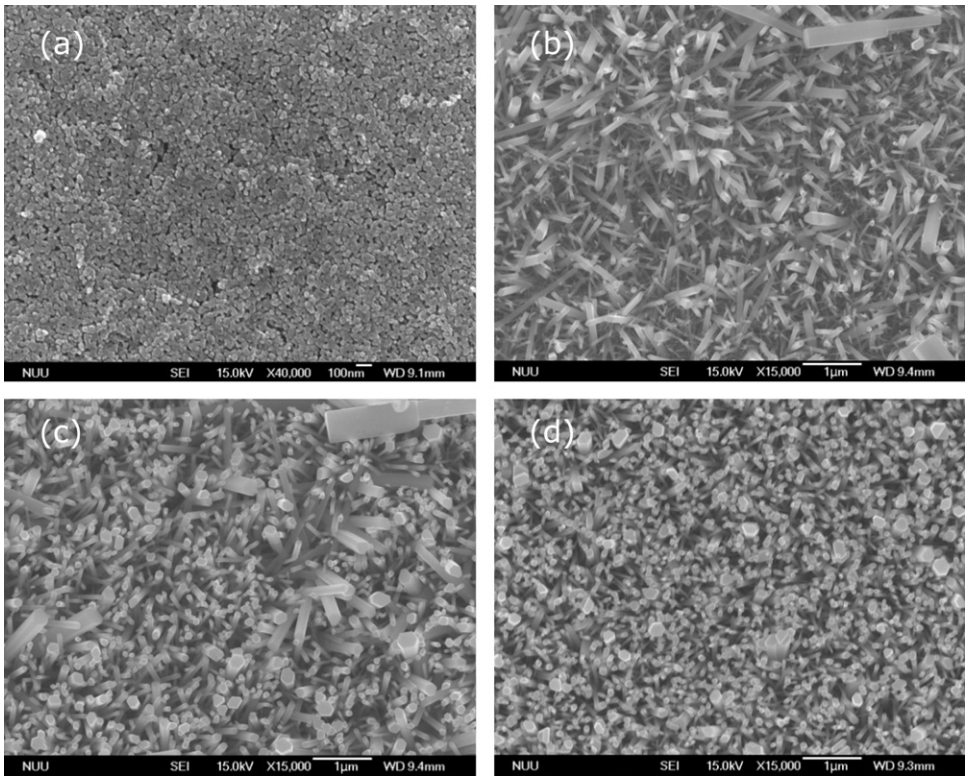

Fig. 3. SEM surface morphology as a function of CBD reaction temperatures. (Deposition time: 3 h; solution concentration: 0.03 M.)

were immersed in an N719 dye at room temperature for 24 h. Cell performance was measured using an electrochemical workstation (Jiehan 5000) under AM 1.5 and 100 mW/cm^2 solar simulator (Peccell, Japan).

3. Results and discussion

3.1. Effects of CBD reaction temperature

The chemical growth of ZnO nanostructures in the solution can be expressed as follows [42,43]

$$C_6H_{12}N_4+6H_2O\rightarrow 6CH_2O+4NH_3 \quad (1)$$

$$NH_3+H_2O\rightarrow NH_4^+ +OH^- \quad (2)$$

$$Zn(CH_3COO)_2+2NH_4^+ +2OH^- \rightarrow 2CH_3COONH_4+Zn(OH)_2 \quad (3)$$

$$Zn^{2+}+2OH^- +2H_2O\rightarrow Zn(OH)_4^{2-}+2H^+ \quad (4)$$

$$Zn(OH)_4^{2-}+2H^+\rightarrow ZnO_{cluster}+3H_2O \quad (5)$$

In the precursor solution, $C_6H_{12}N_4$ serves as a pH buffer by releasing OH^- ions through the thermal decomposition (Eqs. (1) and (2)) [27]. The $Zn(OH)_4^{2-}$ in Eqs. (4) and (5) is the intermediate growth unit, which is transferred into ZnO clusters by the dehydration reaction (Eq. (5)). Here, we first change the reaction temperature from 25 to 95 °C to monitor the ZnO growth during CBD with fixed 0.03 M of the zinc acetate solution. From Fig. 2, the cross-section structures of ZnO prepared at 25, 50, 75 and 95 °C were observed. For reaction temperature above 50 °C, the growth of ZnO branched nanorods and nanorod arrays is observed. Nanostructured ZnO prepared at reaction temperature of 95 °C exhibits highly oriented nanorod arrays; the average length of nanorods is 1.83 μm and the average diameter is around 87 nm. Fig. 3 shows the surface images of the ZnO samples as seen in Fig. 2. It is seen that ZnO was not produced for reaction temperature of 25 °C, while the ZnO nanorod structure was formed at higher reaction temperature (> 50 °C). With increasing the reaction temperature, the density of ZnO nanorods is increased and the uniformity and orientation of ZnO nanorods were also improved. The average diameter of the nanorods is decreased from ~116 to ~87 nm with an increasing temperature, indicating that the diameter is very sensitive to temperature. The XRD and EDS techniques were further used to confirm the nanostructure synthesized by CBD. From Fig. 4(a), the ZnO nanostructures have been grown for reaction temperature above 50 °C, which is coinciding with the SEM results (Figs. 2 and 3). All of the diffraction peaks can be indexed to a wurtzite structure of ZnO [33]. The ZnO nanorods prepared at reaction temperature of 95 °C display the strongest (0 0 2) diffraction peak, revealing that the nanostructures possess well-aligned growth along the *c*-axis direction. Similar results of temperature effect on the growth orientation have been reported for ZnO nanorods grown by the hydrothermal method [44]. The EDS patterns of ZnO nanorods show that oxygen and zinc were only detected elements as seen in Fig. 4(b), and great stoichiometric with the O/(Zn+O) atomic ratio of 0.498 indicates that the ZnO nanorods are stable without an excess adsorption of oxygen and OH radicals. A green emission peak around 520 nm in the PL spectra originated from oxygen vacancies and zinc interstitials was not observed by our CBD [31], which confirms that these ZnO nanorods have high-quality crystalline. Fig. 5 shows the optical transmittance spectra of ZnO samples as a function of CBD reaction temperature. The average optical transmittance is slightly decreased with increasing the reaction time; however, the ZnO nanorod arrays grown at 95 °C still exhibit high-transparency (~80%) in the range 400–800 nm,

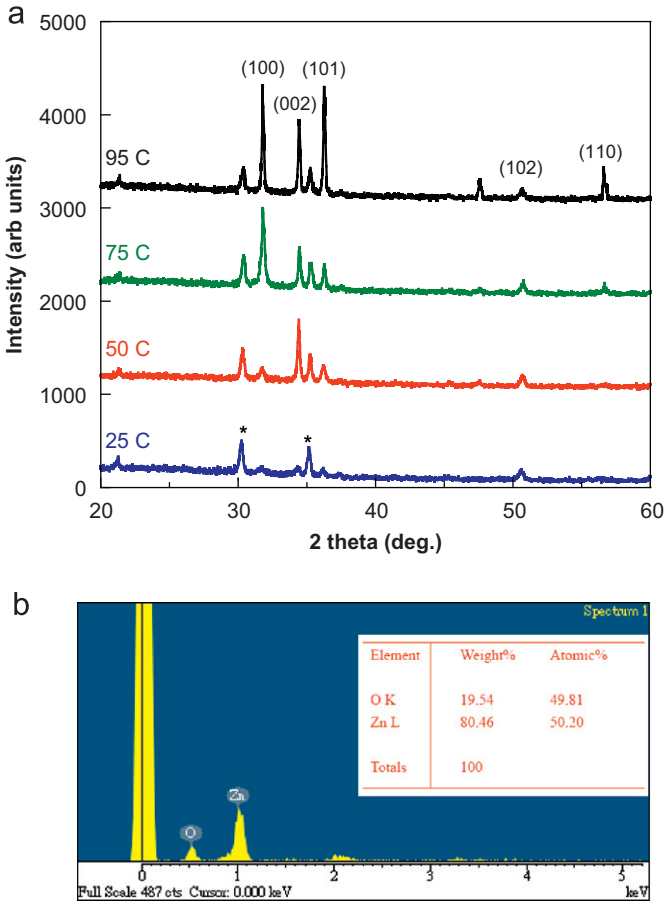

Fig. 4. (a) XRD patterns of the synthesized ZnO as a function of CBD reaction temperatures. The peaks at 30.3° and 35.2° are originated from an ITO substrate. (b) An energy-dispersive X-ray spectroscopy (EDS) spectrum of ZnO nanorods (temperature: 95 °C; solution concentration: 0.03 M).

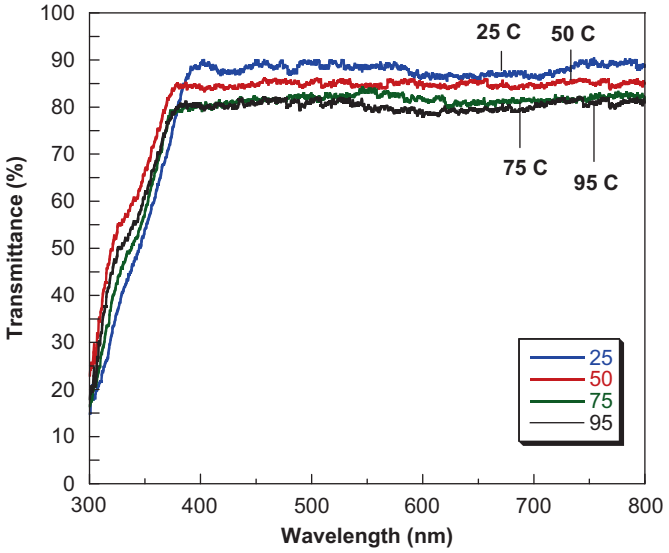

Fig. 5. Optical transmittance spectra of the synthesized ZnO nanorods as a function of CBD reaction temperatures. The substrate is an ITO-glass. (Deposition time: 3 h; solution concentration: 0.03 M.)

due to high crystalline quality [18,36] and high length/diameter aspect ratio. The effect of the higher aspect ratio has been found to enhance light trapping in the solar cell devices with a structure of

ZnO nanorods [17]. The optical bandgap values of the ZnO vary in a rather narrow region (3.28–3.35 eV) determined from $(\alpha h\nu)^{1/2}$ versus photon energy coordinates (not shown).

3.2. Effects of zinc acetate solution concentration

In this section, we investigate the effect of zinc acetate solution concentration on the growth and structural and optical properties of ZnO. The reaction temperature throughout the CBD was set at 95 °C. Fig. 6 shows the SEM surface morphology as a function of solution concentration (0.01–0.1 M). It is observed that the ZnO samples prepared from 0.03 and 0.05 M zinc acetate solution possess highly oriented nanorod arrays with high density, which is due to the fact that the nucleation density on the ITO substrate increases as the Zn concentration in the solution increases. As the solution concentration increases above 0.05 M, it is very obvious that the average diameter is dramatically increased by the clustering of nanorods, which leads to lower aspect ratio and may also worse the degree of nanorod orientation. We further present the cross-section SEM images (Fig. 7) and XRD patterns (Fig. 8) of ZnO to examine the length of nanorods and the orientation degree. The length of the growing ZnO nanorod is in the range 1.8–2.7 μm, and diameter is ranged 43–290 nm (Fig. 6). As evident in Fig. 7, it is clearly seen that ZnO samples grown from 0.01 M zinc acetate solution have shorter length and branched structures. With increasing the solution concentration to 0.03 M, uniform ZnO nanorods were grown, exhibiting highest aspect ratio of ~21 (L~1.83 μm, D~87 nm) and excellent orientation confirmed by the (0 0 2) relative peak intensity as seen in XRD patterns (Fig. 8). This can be explained by the fact that the relatively low concentration of zinc acetate solution corresponds to low concentration of OH^- (Eq. (4)), which provides the higher surface energy for faster growth rate along the c-axis [45]. The reported aspect ratio value is much higher than values of ZnO rods obtained by sol–gel (value: 3–10) [22], CBD (value: ~3.1) [31] or other deposition processes [39,46,47]. It is observed that the aspect ratio of the ZnO nanorods is decreased with the increase of zinc acetate concentration, which is consistent with the previous report [45]. This can be explained that when the concentration is increased, the concentration of OH^- will also increase and then these OH^- ions can partially suppress the growth of as-deposited ZnO nanocrystallines along the c-axis direction [45]. The aspect ratio of ZnO nanostructures prepared by various processes is summarized in Table 1. The comparison of the optical transmittance as a function of solution concentration is shown in Fig. 9. It is observed that the optical transmittance was decreased with an increasing solution concentration. ZnO nanorod arrays prepared from 0.03 M zinc acetate solution still show sufficient high-transparency with an average optical transmittance higher than

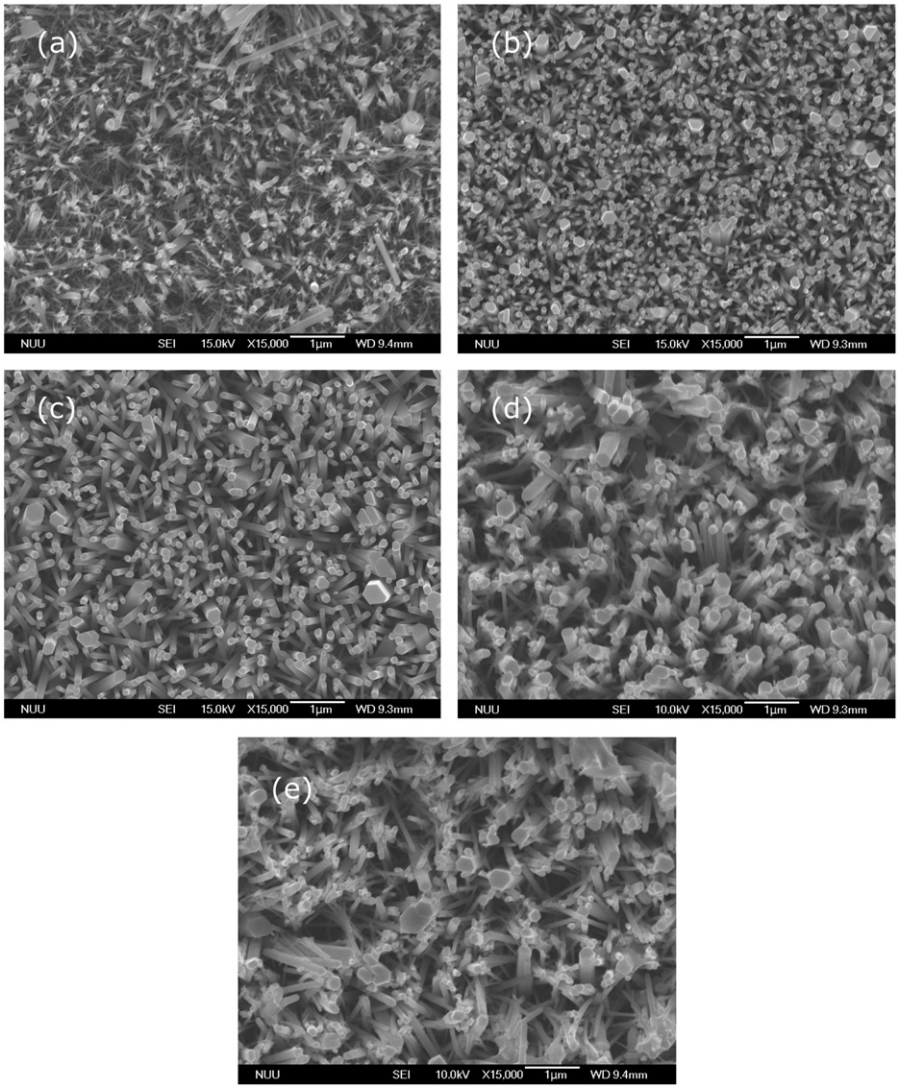

Fig. 6. SEM surface morphology as a function of zinc acetate solution concentration (a–e: 0.01–0.1 M). Growth temperature: 95 °C.

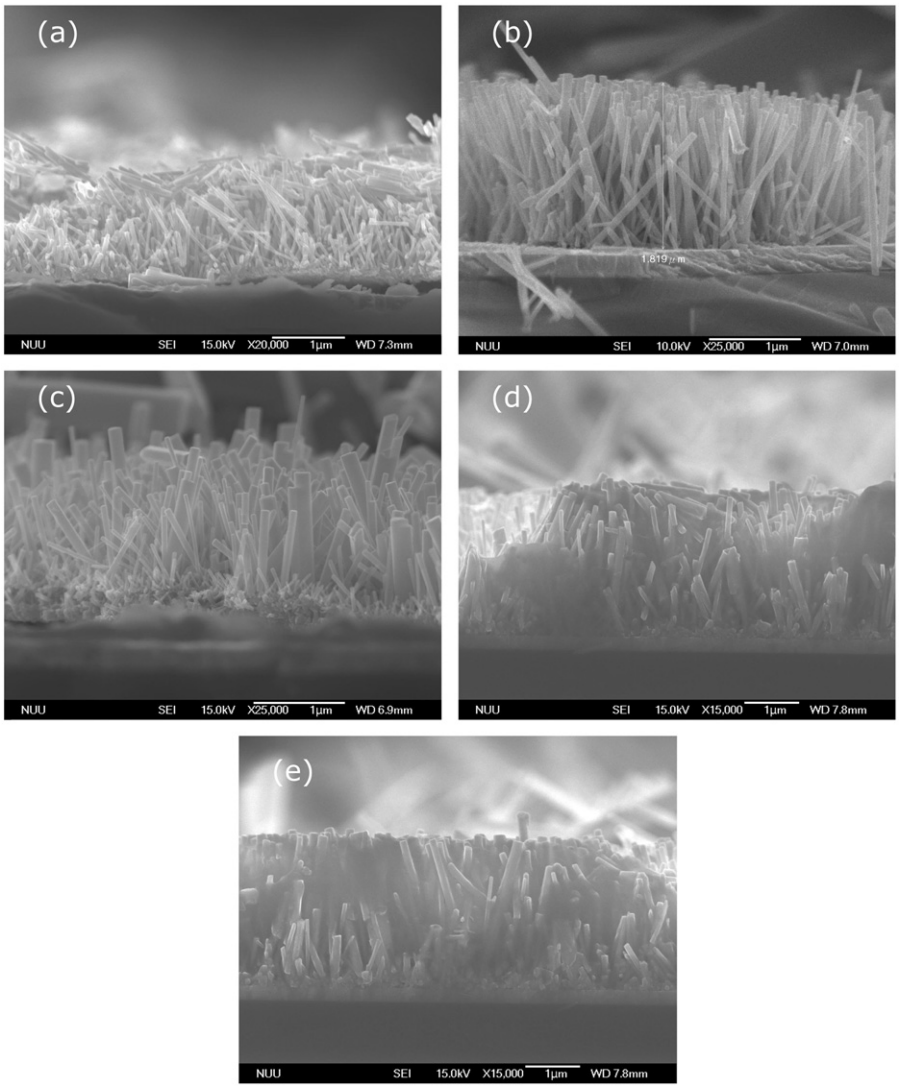

Fig. 7. SEM cross-section images: growth of ZnO nanorods and nanorod arrays as a function of zinc acetate solution concentration (a–e: 0.01–0.1 M). Growth temperature: 95 °C.

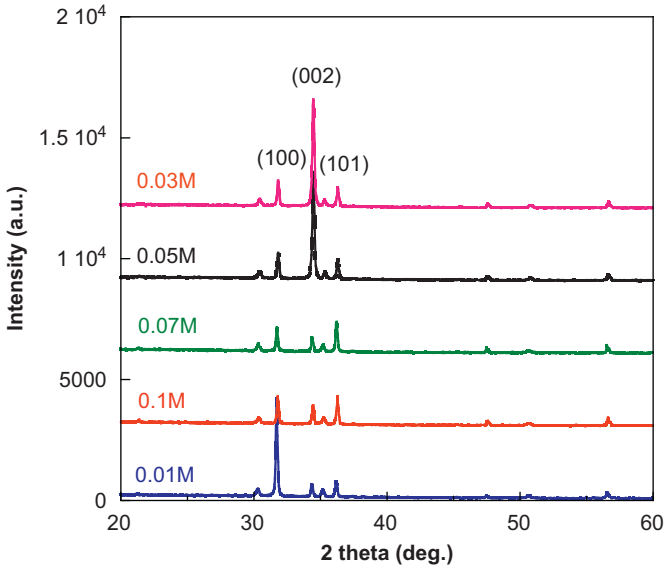

Fig. 8. XRD patterns of the synthesized ZnO as a function of solution concentration. Growth temperature: 95 °C.

Table 1
The aspect ratio (length/diameter) of ZnO nanostructures prepared by various processes.

Substrate	Structure	Aspect ratio	Process
–	Nanorods	1.7–5.6	Solvothermal reaction [46]
Stainless steel	Rods	3.3–4.0	Electrodeposition [39]
ITO	Nanorod arrays	~4	Hydrolysis method [12]
ITO	Nanorods	~4	CBD [31]
–	Nanorods	3–10	sol–gel [22]
PET/ITO	Nanowire arrays	>15	Electrodeposition [45]
Glass	Branched microrod	~16	Solution method [30]
ITO	Nanorod arrays	~21	CBD (this work)

80% in the visible range. The excellent optical property of this ZnO is believed to be attributed to high crystalline quality [21,48], high aspect (length/diameter) ratio and highly oriented nanorod arrays.

3.3. Electrical performance of ZnO/NiO electrode and SS-DSSC

Fig. 10 shows the SEM surface and cross-section morphologies, where the solid ITO/seed layer/ZnO/NiO structure is clearly observed. The typical *I–V* characteristics of the single NiO layer

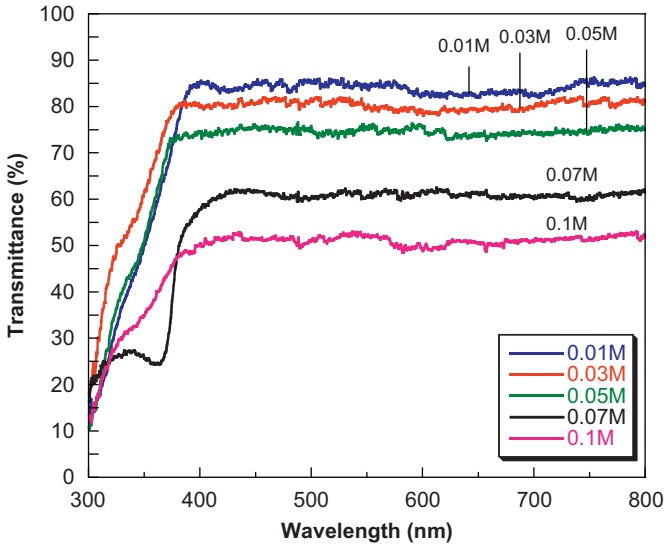

Fig. 9. Optical transmittance spectra of the synthesized ZnO as a function of the solution concentration. The substrate is an ITO-glass. Growth temperature: 95 °C.

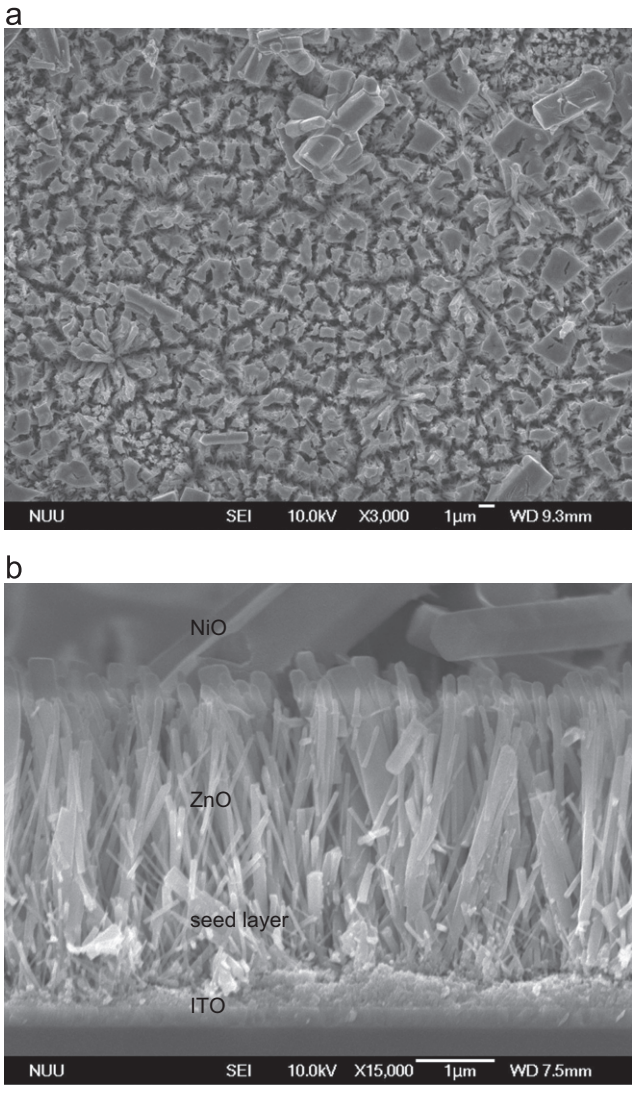

Fig. 10. (a) Surface SEM morphology (top: NiO; underneath: ZnO) and (b) cross-section SEM morphology of ZnO/NiO heterojunction structures.

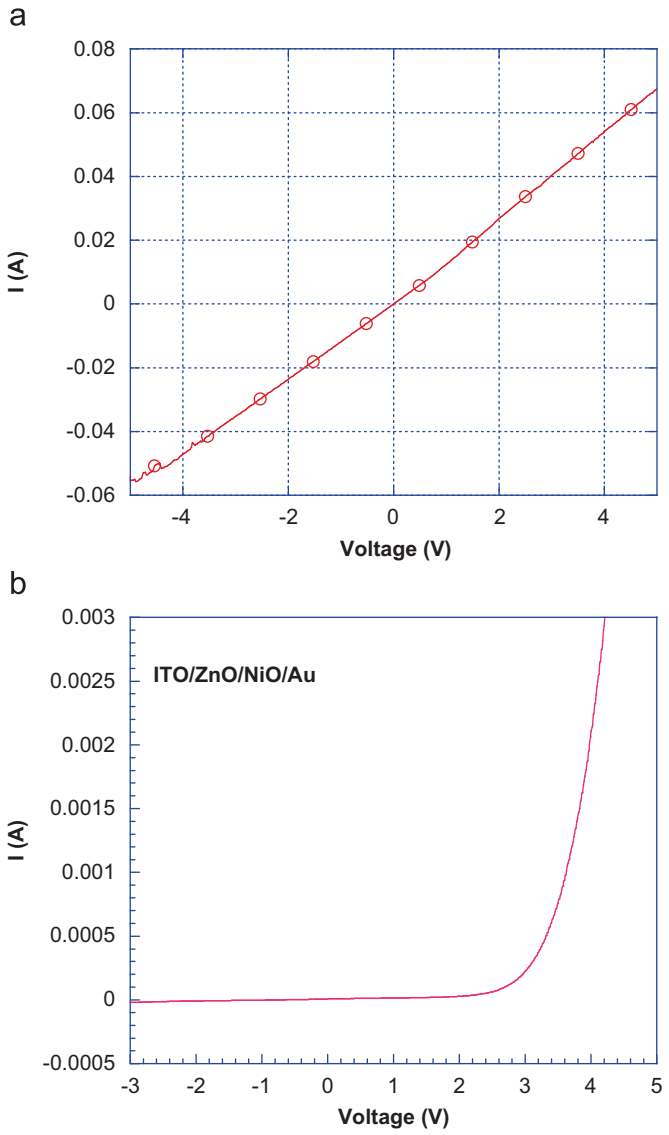

Fig. 11. *I–V* characteristics of (a) ITO/NiO/Au structure and (b) ITO/n-ZnO/p-NiO/Au heterojunction electrode.

and the ZnO/NiO heterojunction at room temperature in the forward and reverse bias conditions are shown in Fig. 11(a) and (b), respectively. The single NiO layer shows a linear *I–V* behavior, indicating that the ohmic contacts are formed between Au counter electrodes and the uniform p-type NiO layer. As seen in Fig. 11(b), the solid heterojunction electrode based on ZnO nanorod arrays exhibited superior rectifying *I–V* characteristics as compared with the n/p heterojunction based on branched ZnO [31] or sputtered-ZnO [49]. This is due to the fact that the ZnO nanorod arrays based heterojunction electrode has low lattice mismatch [50,51], which facilitates electron transport through the n/p interface. It is noted that the reverse leakage current ($\sim 5.6 \times 10^{-5}$ A at -4.5 V) is negligible, revealing that this heterojunction is a solid structure by this two-step CBD method.

Moreover the effects of CBD reaction temperature and solution concentration on the optoelectronic performance of solid-state dye-sensitized solar cells (SS-DSSC) are investigated in details. The SS-DSSCs were constructed of ZnO nanorod arrays/NiO with N719 dye soaking and then measured under the illumination of 100 mW/cm^2 AM 1.5 G simulated sunlight. Fig. 12 reveals the

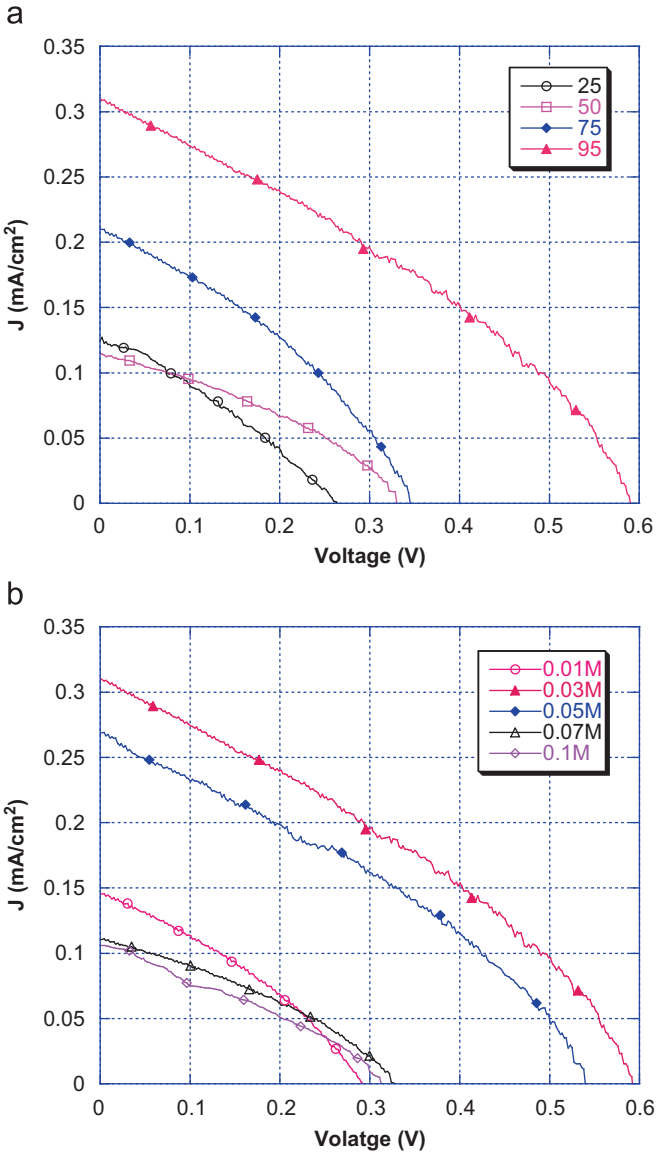

Fig. 12. Current density–voltage (J–V) characteristics of ZnO nanorod arrays based SS-DSSCs as a function of (a) reaction temperature and (b) solution concentration under simulated light, AM. 1.5 and 100 mW/cm^2.

effects of reaction temperature and solution concentration on the I–V characteristics. We observe a trend that the short-circuit current (J_{SC}) and open-circuit voltage (V_{OC}) are significantly increased from 25 to 95 °C, which reflects the increased harvesting of photons. Furthermore, zinc acetate solution concentration also plays a critical role on the cell performance. The best SS-DSSC has J_{SC} of 0.31 mA/cm^2 and V_{OC} of 590 mV for the processing combination of reaction temperature 95 °C and 0.03 M concentration, yielding the maximum conversion efficiency (η) of 0.059%. Compared with the efficiency values (η=0.025–0.032%) of the reported SS-DSSC [41,52], the power conversion efficiency is significantly increased for ZnO nanorod arrays based SS-DSSC under optimization of the array alignment and the aspect ratio value.

4. Conclusion

In summary, this work provides a systematic study of the controlled growth of the ZnO nanorods and nanorod arrays on the ITO substrate by low-temperature chemical bath deposition (CBD). The growth of ZnO nanostructures was clearly observed from the SEM surface and cross-section morphologies as functions of reaction temperature and zinc acetate solution concentration. The growth mechanism involving the formation of intermediate $Zn(OH)_4^{2-}$ growth unit and the subsequent transition into ZnO clusters during the dehydration reaction is remarkably depending on the reaction temperature and the solution concentration. The ZnO nanostructures fabricated under an optimal combination of CBD reaction temperature of 95 °C and solution concentration of 0.03 M show highly aligned nanorod arrays with an average length and diameter of 1.83 μm and 87 nm, respectively. These ZnO nanorod arrays exhibit high aspect ratio of $L/D \sim 21$ and the great crystalline quality, leading to high-transparency ($>80\%$) in the visible wavelength region. The ZnO nanorod arrays based heterojunction (ZnO/NiO) electrode exhibits superior rectifying I–V behavior with extremely low leakage current. Finally, the SS-DSSCs were successfully implemented with the ZnO/NiO heterojunctions under different CBD conditions. It has been shown that the optoelectronic parameters (J_{SC} and V_{OC}) of the cells were significantly influenced by the degree of the nanorod orientation, which can be controlled in the CBD process. The SS-DSSC made of ZnO nanorod arrays with optimal conditions (reaction temperature 95 °C and 0.03 M concentration) has J_{SC} of 0.31 mA/cm^2 and V_{OC} of 590 mV, yielding the maximum conversion efficiency of 0.059%. The results of this work show that the controlled growth of ZnO nanorod arrays such as aspect ratio and/or array alignment by CBD is very promising and stimulating for developing of transparent-conductive electrodes in ZnO based optoelectronic devices.

Acknowledgment

This work was funded through the National Science Council, Taiwan, ROC under Grant no. NSC98-2622-E-239-007-CC3. The financial support is gratefully acknowledged. This work was also partially supported by AGI Corporation under Grant 991009.

References

[1] T. Makino, C. Chia, T. Nguen, Y. Segawa, Applied Physics Letters 77 (2000) 1632.
[2] H. Chik, J. Liang, S. Cloutier, N. Kouklin, J. Xu, Applied Physics Letters 84 (2004) 3376.
[3] T. Ma, M. Guo, M. Zhang, Y.J. Zhang, X.D. Wang, Nanotechnology 18 (2007) 035605.
[4] U. Ozgur, Ya.I. Alivov, C. Liu, A. Teke, M.A. Reshchikov, S. Dogan, V. Avrutin, S.J. Cho, H. Morkoc, Journal of Applied Physics 98 (2005) 041301.
[5] H. Sun, Q.F. Zhang, J.L. Wu, Nanotechnology 17 (2006) 2271.
[6] Y. Xia, P. Yang, Y. Sun, Y. Wu, B. Mayers, B. Gates, Y. Yin, F. Kim, H. Yan, Advanced Materials 15 (2003) 353.
[7] Q. Wan, Q.H. Li, Y.J. Chen, T.H. Wang, X.L. He, J.P. Li, C.L. Lin, Applied Physics Letters 84 (2004) 3654.
[8] H. Cheng, C. Chen, C. Lee, Thin Solid Films 498 (2006) 142.
[9] D. King, R. Nix, Journal of Catalysis 160 (1996) 76.
[10] D. Bagnall, Y. Chen, Z. Zhu, T. Yao, S. Koyama, M. Shen, T. Goto, Applied Physics Letters 70 (1997) 2230.
[11] K. Keis, E. Magnusson, H. Lindstorm, S. Lindquist, A. Hagfelt, Solar Energy Materials and Solar Cells 73 (2002) 51.
[12] R. Thitima, C. Patcharee, S. Takashi, Y. Susumu, Solid-State Electronics 53 (2009) 176.
[13] C.H. Ku, J.J. Wu, Applied Physics Letters 91 (2007) 093117.
[14] D.I. Suh, S.Y. Lee, T.H. Kim, J.M. Chun, E.K. Suh, O.B. Yang, S.K. Lee, Chemical Physics Letters 442 (2007) 348.
[15] D.H. Zhang, T.L. Yang, Q.P. Wang, D.J. Zhang, Materials Chemistry and Physics 68 (2001) 233.
[16] W. Yang, Z. Liu, D. Peng, F. Zhang, H. Huang, Y. Xie, Z. Wu, Applied Surface Science 255 (2009) 5669.
[17] K. Matsubara, P. Fons, K. Iwata, A. Yamada, S. Niki, Thin Solid Films 422 (2002) 176.
[18] J. Lee, K. Ko, B. Park, Journal of Crystal Growth 247 (2003) 119.

[19] L. Yang, Q. Zhao, M. Willander, J. Yang, Journal of Crystal Growth 311 (2009) 1046.
[20] M. Krunks, A. Katerski, T. Dedova, I. Oja Acik, A. Mere, Solar Energy Materials and Solar Cells 92 (2008) 1016.
[21] X. Meng, D. Shen, J. Zhang, D. Zhao, Y. Lu, L. Dong, Z. Zhang, Y. Liu, X. Fan, Solid State Communications 135 (2005) 179.
[22] J. Yang, M. Gao, L. Yang, Y. Zhang, J. Lang, D. Wang, Y. Wang, H. Liu, H. Fan, Applied Surface Science 255 (2008) 2646.
[23] Z. Li, X. Huang, J. Liu, Y. Li, G. Li, Materials Letters 62 (2008) 1503.
[24] M. Law, L.E. Greene, J.C. Johnson, R. Saykally, P.D. Yang, Nature Materials 4 (2005) 455.
[25] E. Galoppini, J. Rochford, H.H. Chen, G. Saraf., Y.C. Lu, A. Hagfeldt, G. Boschloo, Journal of Physical Chemistry B 110 (2006) 16159.
[26] L. Vaysierres, Advanced Materials 15 (2003) 464.
[27] Y.F. Zhu, G.H. Zhou, H.Y. Ding, A.H. Liu, Y.B. Lin, N.L. Li, Physica E 42 (2010) 2460.
[28] X. Li, F. Zhao, J. Fu, X. Yang, J. Wang, C. Liang, M. Wu, Crystal Growth & Design 9 (2009) 409.
[29] S. Mridha, M. Dutta, D. Basak, Journal of Materials Science: Materials in Electronics 20 (2009) S376.
[30] O. Lupan, L. Chow, G. Chai, B. Roldan, A. Naitabdi, A. Schulte, H. Heinrich, Materials Science and Engineering B 145 (2007) 57.
[31] Y.M. Lee, W.M. Nung, C.H. Lai, Physica E 42 (2010) 2289.
[32] L.L. Yang, Q.X. Zhao, M. Willander, J.H. Yang, Journal of Crystal Growth 311 (2009) 1046.
[33] Y.J. Kim, H. Shang, G. Cao, Journal of Sol–Gel Science and Technology 38 (2006) 79.
[34] Y.H. Kang, C.G. Choi, Y.S. Kim, J.K. Kim, Materials Letters 63 (2009) 679.
[35] Z. Li, X. Huang, J. Liu, Y. Li, G. Li, Materials Letters 62 (2008) 1503.
[36] J. Lee, J. Chung, S. Lim, Physica E 42 (2010) 2143.
[37] L. Cao, M.K. Li, M. Lu, W. Zhang, Q. Wei, Z.B. Liu, Materials Science in Semiconductor Processing 11 (2008) 25.
[38] L. Greene, M. Law, D.H. Tan, J. Goldberger, P. Yang, Nano Letters 5 (2005) 1231.
[39] A.E. Rakhshani, Applied Physics A 92 (2008) 303.
[40] Y.M. Lee, C.H. Hsu, H.W. Chen, Applied Surface Science 255 (2009) 4658.
[41] Y.M. Lee, C.H. Lai, Solid-State Electronics 53 (2009) 1116.
[42] H.W. Hou, Y. Xie, Q. Li, Solid State Science 7 (2005) 45.
[43] M. Wang, C. Ye, Y. Zhang, G. Hua, H. Wang, M. Kong, L. Zhang, Journal of Crystal Growth 291 (2006) 334.
[44] M. Guo, P. Diao, S. Cai, J. Solid, State Chemistry 178 (2005) 1864.
[45] X.Y. Kong, Z.L. Wang, Applied Physics Letters 84 (2004) 975.
[46] O. Lupan, T. Pauporte, Journal of Crystal Growth 312 (2010) 2454.
[47] P. Tonto, O. Mekasuwandumrong, S. Phatanasri, V. Pavarajarn, P. Praserthdam, Ceramics International 34 (2008) 57.
[48] C.H. Ahn, S.K. Mohanta, N.E. Lee, H.K. Cho, Applied Physics Letters 94 (2009) 261904.
[49] J. Huang, L.J. Wang, R. Xu, K. Tang, J.M. Lai, J. Wang, Y.Y. Lou, W.M. Shi, Y.B. Xia, Journal of Physics: Conference Series 152 (2009) 012017.
[50] H. Ohta, M. Hirano, K. Nakahara, H. Maruta, T. Tanabe, M. Kamiya, T. Kamiya, H. Hosono, Applied Physics Letters 83 (2003) 1029.
[51] H.L. Chen, Y.S. Yang, Thin Solid Films 516 (2008) 5590.
[52] J. Bandara, H. Weerasinghe, Solar Energy Materials and Solar Cells 85 (2005) 385.